Biophysical Journal, Volume *122*

Supplemental information

Differential regulation of GUV mechanics via actin network architectures

Nadab H. Wubshet, Bowei Wu, Shravan Veerapaneni, and Allen P. Liu

Supplementary Information for

Differential regulation of GUV mechanics via actin network architectures

Nadab H. Wubshet, Bowei Wu, Shravan Veerapaneni, Allen P. Liu

Corresponding author: Allen P. Liu
Email: allenliu@umich.edu

This PDF file includes:

Supplementary text
Figures S1 to S7
Tables S1 to S2
Legends for Movies S1 to S6
SI References

Other supplementary materials for this manuscript include the following:

Movies S1 to S6

Supplementary Information Text

Numerical method

The parameters used in this numerical analysis are summarized in **Table S1**. Consider a GUV comprised of charge-free bilipid membrane with its interior and exterior filled with a fluid of viscosities μ_{in} and μ_{ex} respectively. To model the electrohydrodynamics, we will employ the leaky dielectric model (1), which combines the Ohm's law for electric current conservation and the Stokes equations for fluid motion. The fluid velocity u satisfies

$$-\mu\nabla p + \Delta \boldsymbol{u} = 0, \quad \nabla \cdot \mathbf{u} = 0,$$

in the interior and exterior of the vesicles subject to a far-field condition and a no-slip boundary condition at the GUV boundary γ. In addition, at γ, the membrane elastic forces balance the electric and hydrodynamic forces, that is, $\mathbf{f}_{mem} = \mathbf{f}_{el} + \mathbf{f}_{hd}$. The membrane elastic forces are obtained by taking the gradient of the Helfrich energy, $E_m = \frac{1}{2}(\int_\gamma \kappa_b \kappa^2 d\gamma)$, that is used for modeling the membrane energy. Here, κ_b is the bending modulus and κ is the planar membrane curvature. The local inextensibility of the membrane is enforced by letting the surface divergence of the interfacial velocity vanish, that is,

$$\nabla\gamma \cdot \dot{\boldsymbol{x}} = 0,$$

where **x** is assumed to be the position of the interface. This constraint will be enforced via augmented Lagrangian approach. Thereby, it gives rise to an additional interfacial force due to tension λ, the Lagrange multiplier. The combined expression is given by,

$$\boldsymbol{f}_{el} = -\kappa_b \left(\kappa_{ss} + \frac{\kappa^3}{2}\right)\boldsymbol{n} + (\lambda \boldsymbol{x}_s)_s,$$

where **n** is the outward normal to vesicle interface. The remaining component we require to close the system of equations for vesicle EHD is the electric force $\mathbf{f}_{el}$ acting on the fluid. It is given by the jump in the normal component of the Maxwell stress tensor:

$$\boldsymbol{f}_{el} = \left[\left[\boldsymbol{n} \cdot \left(\epsilon \boldsymbol{E} \otimes \boldsymbol{E} - \frac{1}{2}\epsilon \left|\left|\boldsymbol{E}\right|\right|^2 \boldsymbol{I}\right)\right]\right],$$

where ε is the permittivity, **E** is the electric field and [·] is the difference between interior and exterior fields. The ambient electric field is conservative and can be computed from the electric potential, $\mathbf{E} = -\nabla\varphi$, by solving the Laplace equation, $-\Delta\varphi = 0$, in the interior and exterior of the vesicle interface. The boundary conditions at the fluid-membrane interface are obtained by charge and current conservation across the membrane (2). The charge accumulation is governed by: (i) Charge convection by the fluid motion along the surface, (ii) Membrane conductance, with strength G_m, arising from the presence of pores, pumps and ion channels. (iii) Membrane capacitance C_m. Together, the interfacial conditions can be written as

$$\left[\left[\sigma E_n + \epsilon \dot{E}_n\right]\right] = 0$$

$$C_m \dot{V}_m + G_m V_m = \sigma_{ex} E_{n,ex} + \epsilon_{ex} \dot{E}_{n,ex}$$

where σ is the fluid conductivity, E_n is the normal electric field at the membrane interface and $V_m = [[\varphi]]$ is the potential difference across the membrane. The values used for this numerical analysis are summarized in **Table S2**.

In summary, given the initial shape of a GUV, we need to solve for the electric potential and the fluid velocity at the interface, advance the interface position via the kinematic condition, and update the membrane electric variables using (3). We employ the boundary integral formulation developed in (4) for solving the Stokes equations and that of (3,5) for the electric potential problem, with appropriate modifications to account for the imposed AC electric field (as opposed to DC field considered in those works).

Dimensionless parameters used for numerical simulation

Outer solution property
ε_{ex} of 200mM glucose = 79.4 (6) absolute ε_{ex} = 7.03 x 10^{-10}
σ_{ex} of 200 mM glucose = 0.179 mS/m (6)
μ_{ex} of 200 mM glucose = 1mPa.s (7)

Membrane property
C_m = 1μF/cm^2 (8)
A ~10 μm
G_m = 0, assuming intact lipids (8)
κ = 10^{-19} J

Applied Electric field
E_o = 30 kV/m
ω = 5 kHz

Inner solution property (PEG8000 2%, 4%, 8%)
ε_{in} PEG8000 = 80.2, absolute ε_{ex} = 7.1 x 10^{-10}
μ_{in} of 2% PEG = 1.05 mPa.s
μ_{in} of 4% PEG = 3.02 mPa.s
μ_{in} of 8% PEG = 6.94 mPa.s (9)

σ_{in} of 2% PEG = 16.7 dS/cm
σ_{in} of 4% PEG = 14.1 dS/cm
σ_{in} of 8% PEG = 11.7 dSc/m (10)

Electrical conductivity values of aqueous PEG 8000 solutions were acquired from Burnett et. al. (10). In this article, electrical conductivity of PEG 8000 was measured for various PEG 8000 concentrations in Hoagland solution. Within the range of 0-10% w/v PEG8000 concentration, electrical conductivity was measured to have a linear correlation with PEG8000 concentration. To calculate the conductivity of PEG 8000 dissolved in water, we linearly interpolated for unknown values of x% w/v PEG8000 electrical conductivity in water using electrical conductivity of water and Hoagland solution as the independent variables.

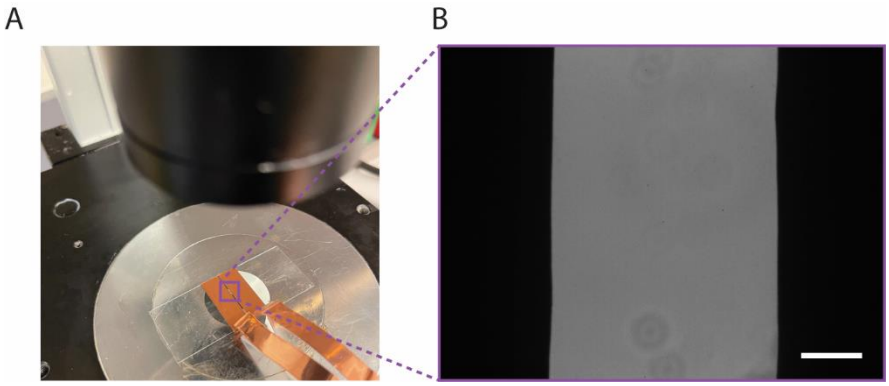

Fig. S1. Electrodeformation chamber. (A) Electrodefomation chamber made by using copper tapes that are parallelly spaced and uniformly adhered to a coverslip glass. (B) Electrodeformation chamber image acquired using a 20X objective. Dark regions on both sides indicate copper electrodes. Scale bar is 50 μm.

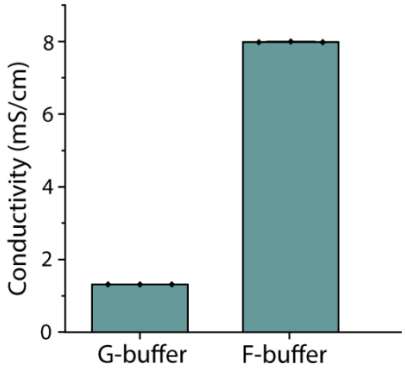

Fig. S2. Measured conductivity of buffers used to reconstitute globular actin (G-actin) and filamentous actin (F-actin). Mean ± standard deviation, n = 3.

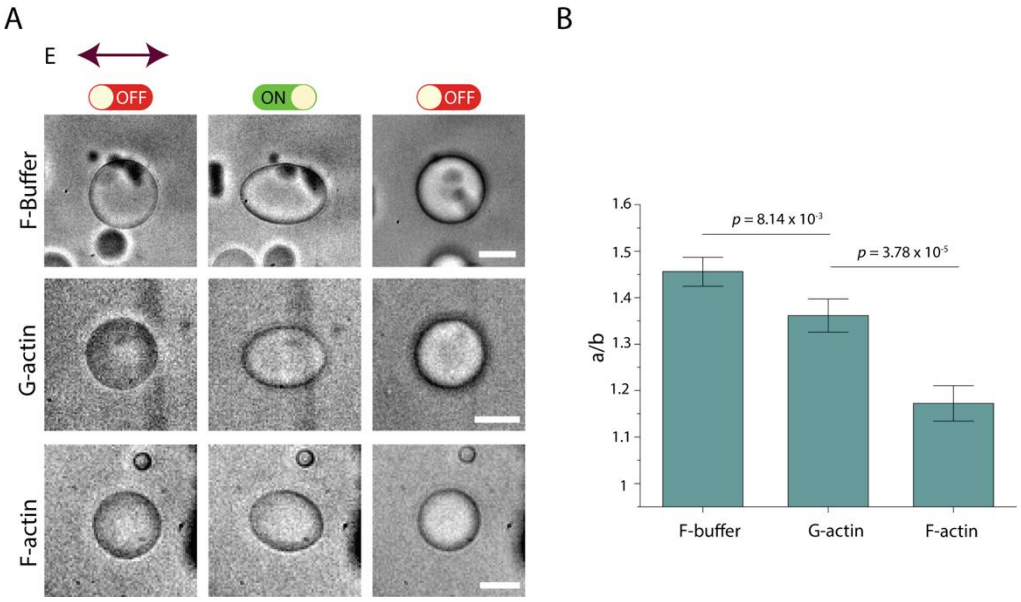

Fig. S3. Electrodeformation of GUVs containing F-buffer, 5.3 µM G-actin in G-buffer and 5.3 µM F-actin in F-buffer. (A) Brightfield images show transformation of GUVs from unperturbed (left column) to elliptically electrodeformed during application of electric field (middle column) to spherical recovery (right column). F-buffer (top), G-actin (middle), and F-actin (bottom) are compared. (B) Maximum a/b ratio of GUVs from the three conditions indicated. Data represent mean maximum deformation and error bars denote ± SE. $N_{F\text{-buffer}} = 11$, $N_{G\text{-actin}} = 13$, $N_{F\text{-actin}} = 12$. Scale bars, 10 µm.

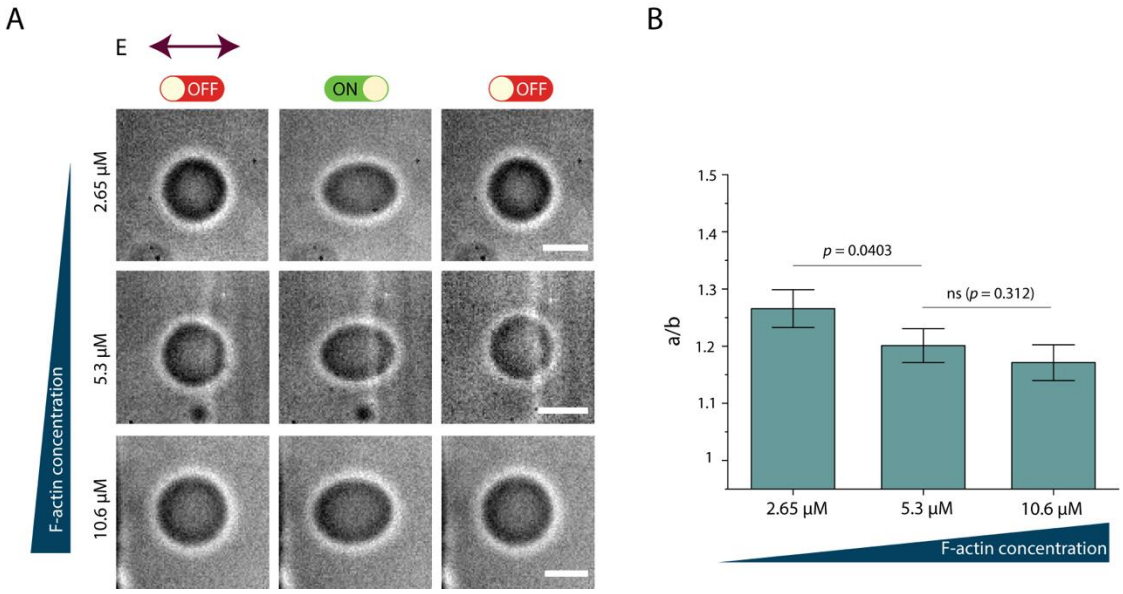

Fig. S4. Electrodeformation of GUVs encapsulating F-actin at varying actin concentrations. (A) Brightfield images show transformation of GUVs from unperturbed (left column) to elliptically electrodeformed during application of electric field (middle column) to spherical recovery (right column). Images of GUVs with 2.65 µM (top), 5.3 µM (middle), and 10.6 µM (bottom) actin are displayed. (B) Maximum a/b ratio of GUVs from the three conditions indicated. Data represent mean maximum deformation and error bars denote ± SE. $N_{2.65\ \mu M}$ = 12, $N_{5.3\ \mu M}$ = 12, $N_{10.6\ \mu M}$ = 11. Scale bars, 10 µm.

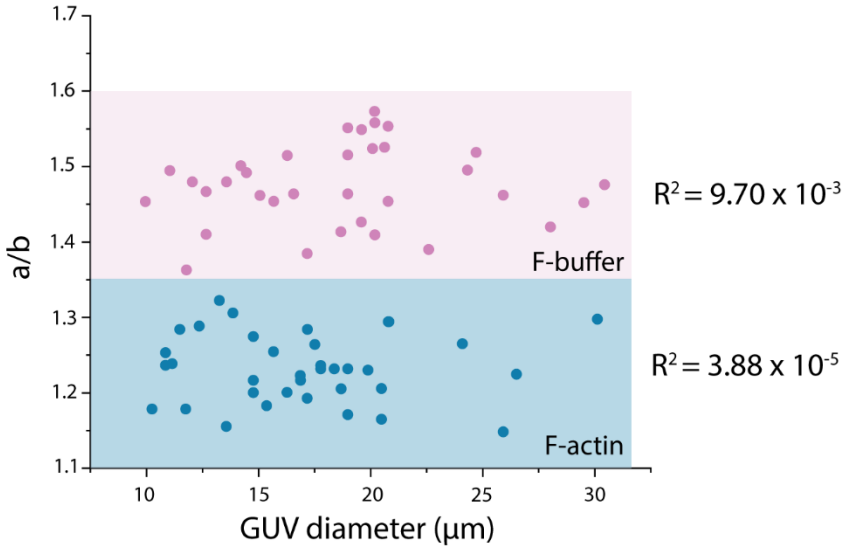

Fig. S5. Lack of correlation between GUV size and steady-state GUV deformation during electroperturbation for both GUVs with F-buffer and with 5.3 µM F-actin. Blue data points and shaded area indicate GUV population encapsulating F-actin and pink data points and shaded area indicate GUV population encapsulating F-buffer. $N_{F\text{-}actin} = 32$, $N_{F\text{-}buffer} = 30$.

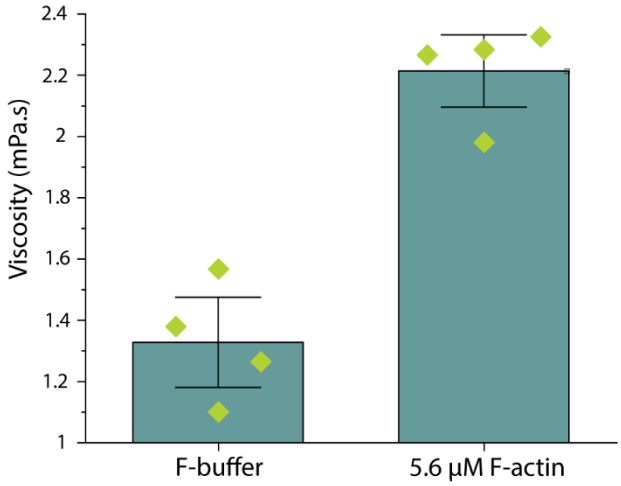

Fig. S6. Measured viscosity of actin polymerization buffer (F-buffer) and 5.3 µM F-actin. Mean ± standard deviation, n = 4.

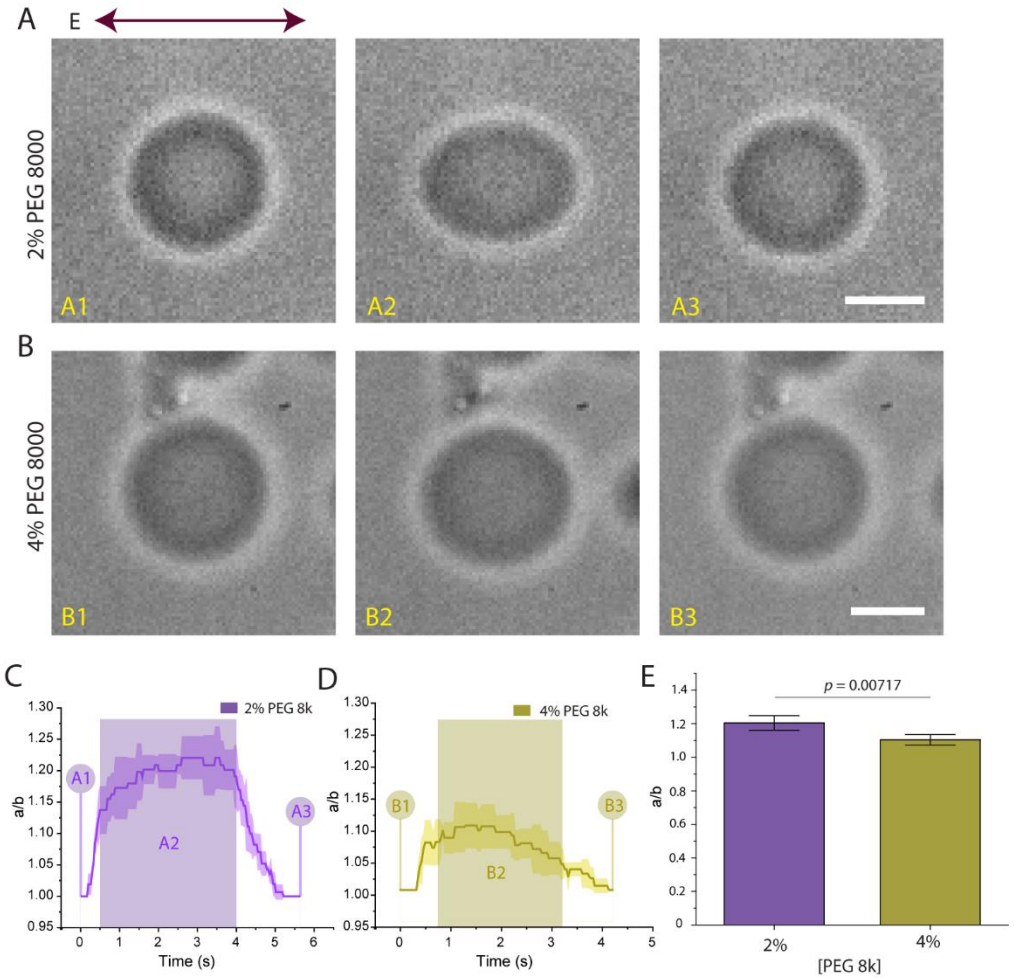

Fig. S7. Electroperturbation of GUVs at variable viscosity contrast (η) with a fixed conductivity ratio Λ. (A) A sequence of brightfield images shows transformation of 2% PEG 8000 encapsulating GUVs from spherical (A1) to prolate deformed (A2) back to spherical recovery (A3). (B) Electrodeformation of 4% PEG 8000 encapsulating GUVs. Conductivity ratio Λ was matched to that of 2% PEG 8000 by addition of 7.5 mM NaCl. (C,D) Deformation profile of 2 or 4% PEG 8000-containing GUVs in response to 30 kV/m AC field. (E) Comparison and statistical analysis of maximum GUV deformation of each GUV condition as indicated. Data represent mean maximum deformation and error bars denote ± SE. $N_{2\%}$= 10, $N_{4\%}$ = 10. Scale bars, 10 µm.

Table S1. Appendix of parameters used in numerical analysis of vesicle electroperturbation

Parameters	**Description**
ε_{ex}	Inner solution permittivity
ε_{in}	Outer solution permittivity
σ_{ex}	Outer solution conductivity
σ_{in}	Inner solution conductivity
μ_{in}	Inner solution dynamic viscosity
μ_{ex}	Outer solution dynamic viscosity
C_m	Membrane capacitance
a	Vesicle radius
E_o	Electric field strength
ω	Frequency
G_m	Membrane conductivity
κ	Membrane bending modulus

Table S2. List of dimensionless parameters

Dimensionless parameter	**Equation**	**Description**	**Value for (PEG8000 2%, 4%, 8%)**
β	$\boldsymbol{\varepsilon_{ex}E_o^2aC_m/\mu_{ex}\sigma_{ex}}$	Electric field strength	0.99162
χ	$\boldsymbol{C_m\kappa/\sigma_{ex}\mu_{ex}a^2}$	Bending rigidity	$0.559\text{x}10^{-4}$
G	$\boldsymbol{aG_m/\sigma_{ex}}$	Membrane conductivity	0
α	$\boldsymbol{\varepsilon_{ex}/aC_m}$	Bulk charge relaxation time	$7.1\text{x}10^{-3}$
Λ	$\boldsymbol{\sigma_{in}/\sigma_{ex}}$	Conductivity ratio	0.93, 0.79, 0.65
η	$\boldsymbol{\mu_{in}/\mu_{ex}}$	Viscosity ratio	1.05, 3.02, 6.94
ξ	$\boldsymbol{\varepsilon_{in}/\varepsilon_{ex}}$	Dielectric permittivity ratio	1.01
Ω	$\boldsymbol{\omega aC_m/\sigma_{ex}}$	AC field frequency	2.79

Supplementary Movie

Movie S1 (separate file). Bright-field image series of electrically perturbed GUVs acquired using a high-speed camera at 400 fps. Prolate deformation of GUVs achieved by encapsulating solution with electrical conductivity ratio $\Lambda > 1$ and applying 30 kV/m AC field at 5 kHz frequency. Scale bar, 10 µm.

Movie S2 (separate file). Bright-field image series of oblate GUV deformation in response to electrical perturbation. Oblate deformation mode was achieved by encapsulating solution with electrical conductivity ratio $\Lambda < 1$ and applying 30 kV/m AC field at 50 kHz frequency. Scale bar, 10 µm.

Movie S3 (separate file). Confocal image series of electrically perturbed actin filament GUVs acquired every 170 ms. Green, ATTO 488 actin. Scale bar, 10 µm.

Movie S4 (separate file). Bright-field image series of 2% PEG 8000 encapsulating GUVs acquired using a high-speed camera at 400 fps. Scale bar, 10 µm.

Movie S5 (separate file). Electrodeformation of GUVs encapsulating 4% PEG 8000. Scale bar, 10 µm.

Movie S6 (separate file). Electrodeformation of GUVs encapsulating 8% PEG 8000. Scale bar, 10 µm.

SI References

1. Melcher JR, Taylor GI. Electrohydrodynamics: a review of the role of interfacial shear stresses. Annu Rev Fluid Mech. 1969;1(1):111–46.
2. Vlahovska PM, Gracià RS, Aranda-Espinoza S, Dimova R. Electrohydrodynamic model of vesicle deformation in alternating electric fields. Biophys J. 2009;96(12):4789–803.
3. Wu B, Veerapaneni S. Electrohydrodynamics of deflated vesicles: budding, rheology and pairwise interactions. J Fluid Mech. 2019;867:334–47.
4. Rahimian A, Veerapaneni SK, Biros G. Dynamic simulation of locally inextensible vesicles suspended in an arbitrary two-dimensional domain, a boundary integral method. J Comput Phys. 2010;229(18):6466–84.
5. Veerapaneni S. Integral equation methods for vesicle electrohydrodynamics in three dimensions. J Comput Phys. 2016;326:278–89.
6. Yoon G. Dielectric properties of glucose in bulk aqueous solutions: Influence of electrode polarization and modeling. Biosens Bioelectron. 2011;26(5):2347–53.
7. Telis VRN, Telis-Romero J, Mazzotti HB, Gabas AL. Viscosity of aqueous carbohydrate solutions at different temperatures and concentrations. Int J food Prop. 2007;10(1):185–95.
8. McConnell LC, Vlahovska PM, Miksis MJ. Vesicle dynamics in uniform electric fields: squaring and breathing. Soft Matter. 2015;11(24):4840–6.
9. Gonzalez-Tello P, Camacho F, Blazquez G. Density and viscosity of concentrated aqueous solutions of polyethylene glycol. J Chem Eng Data. 1994;39(3):611–4.
10. Burnett S, van Iersel M, Thomas P. PEG-8000 alters morphology and nutrient concentration of hydroponic impatiens. HortScience. 2005;40(6):1768–72.